OPTICAL REVIEW Vol. 10, No. 6 (2003) 567–571

Process Algorithms for Resolution Improvement and Contrast Enhancement in Optical Coherence Tomography

I-Jen HSU, Chia-Wei SUN, Chih-Wei LU, Chih-Chung YANG*, Chun-Ping CHIANG[1], Chii-Wann LIN[2]

Graduate Institute of Electro-Optical Engineering and Department of Electrical Engineering, National Taiwan University, 1, Roosevelt Road, Section 4, Taipei, Taiwan, R.O.C.

[1]*Department of Dentistry, National Taiwan University, 1, Roosevelt Road, Section 4, Taipei, Taiwan, R.O.C.*

[2]*Graduate Institute of Bioengineering, National Taiwan University, 1, Roosevelt Road, Section 4, Taipei, Taiwan, R.O.C.*

(Received March 6, 2003; Accepted October 9, 2003)

We proposed two process algorithms for resolution improvement and contrast enhancement in the images of optical coherence tomography (OCT). An OCT system with a non-Gaussian light source spectrum or dispersion mismatch usually results in sidelobes in the interference fringe envelope that may produce artifacts and reduce image contrast. Based on the concept of deconvolution, we proposed two different process algorithms and demonstrated their effectiveness in retrieving sample structures. The effects of the process algorithms were examined by numerical simulations and real OCT scanning images. After processing with the proposed procedures, the effects of sidelobes were tremendously suppressed and the image qualities were improved.

Key words: optical coherence tomography, process algorithm, image resolution, image contrast, deconvolution

1. Introduction

Optical coherence tomography (OCT) is a noninvasive imaging technique and has been widely studied for biomedical applications.[1)] Because the longitudinal resolution of an OCT system is inversely proportional to the spectral width of its light source, broadband light sources are required for high-resolution OCT systems. Current developments for improving the spatial resolution of OCT systems by use of ultra-broadband light sources include the use of a photonic crystal fiber in combination with a compact sub-10 fs Ti:sapphire laser to generate a spectrum ranging from 550 to 950 nm. This broad spectrum results in submicrometer axial resolution in an OCT system.[2)] Also, the use of a spectral continuum from 800 to 1400 nm generated from a photonic crystal fiber to produce longitudinal resolution of 1.3-μm in biological tissue was reported.[3)] Meanwhile, a continuum generation through an ultrahigh-numerical-aperture fiber,[4)] and a superluminescent light source using a Ti:Al_2O_3 crystal pumped by a frequency doubled diode-pumped laser[5)] were used for high-resolution OCT systems.

Although an ultra-broadband light source can result in ultra-high resolution in an OCT system, it usually has a non-Gaussian spectrum and produces sidelobes in the interference fringe envelope. The sidelobes can be suppressed by shaping the spectrum into a Gaussian form. However, such a process will reduce the spectral width and degrade the longitudinal resolution of the OCT system. If appropriate process algorithms can be applied to suppress the sidelobes in the interference fringe envelope, the ultra-broadband light source can be used without spectral shaping and the ultra-high resolution of the OCT system can be preserved. Several signal-processing methods have been developed to increase the resolution of OCT images, such as deconvolution with the iterative restoration algorithms[6–8)] and reduction of the sidelobes with a spectral shaping technique.[9)]

In this paper, we propose and demonstrate two different process algorithms to improve the resolution and to enhance the contrast of OCT images. The effects of these algorithms are demonstrated with numerical simulations and shown with real OCT scanning images. The applicability and limitation of the process algorithms are also discussed. In section 2 of this paper, the concepts of the proposed algorithms are discussed, and their procedures are described in section 3. The results of numerical simulations are presented in section 4. Application of the proposed algorithms to practical OCT scanning results is shown in section 5. Finally, conclusions and discussion are given in section 6.

2. Concepts of the Process Algorithms

An OCT image is a collection of A-scan signals that are obtained from the distributions of interference patterns of photons backscattered by the interfaces of the sample interfering with the photons from the reference arm. The detected signal in an A-scan is

$$\begin{aligned} I(\tau) &= \left\langle \left| \left(\sum_i E_1(t+\tau_i) \right) + E_2(t+\tau) \right|^2 \right\rangle \\ &= I_1 + I_2 + 2\,\mathrm{Re} \sum_i \langle E_1(t+\tau_i) E_2^*(t+\tau) \rangle . \end{aligned} \tag{1}$$

Here, E_1 and E_2 stand for the wave fields from the sample and reference arms, respectively, and I_1 and I_2 are the intensities in the two arms. They are defined as

$$I_1 = \left\langle \left| \sum_i E_1(t+\tau_i) \right|^2 \right\rangle, \tag{2}$$

$$I_2 = \langle |E_2(t)|^2 \rangle . \tag{3}$$

The time delay τ is measured between the reflection at the mirror in the reference arm and that at the first interface of the sample. τ_i denotes the time delay of the photons from the ith interface of the sample relative to those from the first interface. The first two terms in Eq. (1) correspond to dc components during scan and will be neglected in the

*E-mail address: ccy@cc.ee.ntu.edu.tw

following discussion. For a light source with the spectral function $S(\omega)$, the wave field can be expressed as the inverse-Fourier transform of the spectral function as

$$E(t) = \frac{1}{2\pi}\int_{-\infty}^{\infty} S(\omega)\exp[j\phi(\omega)]\exp(j\omega t)\mathrm{d}\omega. \quad (4)$$

Here, $\phi(\omega)$ represents the frequency-dependent phase. The one-dimensional OCT scanning signal obtained from a single-facet reflection in the sample arm is related to the autocorrelation function

$$\begin{aligned}\Gamma(\tau) &= \int_{-\infty}^{\infty} E_1(t)E_2^*(t+\tau)\mathrm{d}t \\ &= \frac{1}{2\pi}\int_{-\infty}^{\infty} |S(\omega)|^2\exp(-j\omega\tau)\mathrm{d}\omega.\end{aligned} \quad (5)$$

We assume that the dispersion between the sample and reference arms is balanced and the spectrum is not modified in either arm. For a sample with multiple interfaces, the interference term of the detected signal will be

$$I(\tau) = \frac{1}{\pi}\mathrm{Re}\sum_i A_i\int_{-\infty}^{\infty}|S(\omega)|^2\exp[-j\omega(\tau-\tau_i)]\mathrm{d}\omega, \quad (6)$$

where A_i is the amplitude fraction of wave field scattered from the ith interface of the sample. If we consider a Gaussian spectrum with the spectral density

$$|S(\omega)|^2 = S_0^2\exp\left[-\left(\frac{\omega-\omega_0}{\Delta\omega}\right)^2\right], \quad (7)$$

the detected signal in Eq. (6) becomes

$$\begin{aligned}I(\tau) = \frac{S_0^2\Delta\omega}{\sqrt{\pi}}\sum_i A_i\exp\left[-\frac{\Delta\omega^2(\tau-\tau_i)^2}{4}\right] \\ \times\cos[\omega_0(\tau-\tau_i)].\end{aligned} \quad (8)$$

A one-dimensional OCT image is obtained from the envelope of the detected signal after demodulation of the carrier frequency. The detected signal can be regarded as a superposition of interference fringe patterns with different amplitudes at different depths. When the distances between the two neighboring interfaces of the sample are larger than the widths of the individual interference fringe envelopes, the demodulated signal is approximately a convolution of the function describing the sample structure and the normalized interference fringe envelope of a single-facet reflection. Under this approximation, the demodulated detected signal can be expressed as

$$I_i = \sum_{i=1}^{N} I'_j f_{i-j}. \quad (9)$$

Here, i and j denote the discrete coordinates that represent the depths in the sample, and N is the pixel number. In comparison with the undemodulated signal described in Eq. (8), I' corresponds to the coefficient including A_i, and represents the intensity that describes the sample structure. The function f corresponds to the exponential factor in Eq. (8) and stands for the normalized interference fringe envelope of a single-facet reflection. f_0 is defined as the peak and has the value 1. The first step of our process algorithm is to find a certain function as an assumed sample structure to be the initial guess in the procedure of iterations. The function of the assumed sample structure is then modified to approach the real one by comparing the demodulated detected signal to the result of convolving the assumed function with the normalized interference fringe envelope of a single-facet reflection. Note that when the distance between two neighboring interfaces in the sample is less than the width of the individual interference fringe envelope, the two interference fringe patterns overlap. In this situation, the demodulated signal cannot be simply considered as a convolution of the sample structure function and the normalized interference fringe envelope of a single-facet reflection. Therefore, the proposed algorithms can be used only when the separation between two neighboring structure features in a sample is not much smaller than the resolution cell size. The applicability and the limitation of the algorithms will be discussed in the next section.

3. Procedures of the Process Algorithms

We propose two different methods for constructing the assumed function as the initial guess of iterations. The flowchart of the first method is shown in Fig. 1(a). With the definition in Eq. (9), the detected intensities at various pixels $I_1 \sim I_N$ are constructed to form a vector I. The relevant parts of the function f are constructed to form the vectors $f_1 \sim f_N$. The inner product of f_i and I, namely, J_i (see Fig. 1(a)), is exactly the ith component of the convolution of functions I and f. The initial function I' is obtained by dividing the detected intensity I by r, where r is the ratio of the maximum values of J_i and I_i. In the second method, the initial guess function is constructed with the local maximum of the detected intensity I. Its flowchart is shown in Fig. 1(b). The value of the initial guess function at any pixel I'_i is set equal to I_i when I_i is a local maximum and set to 0 at other pixels.

The constructed initial guess function is then processed with the procedure described in Fig. 2. Here, I''_i is the inner product of f_i and I', and is the ith component of the convolution of the initial guess function I' and f. The difference between I'' and the detected intensity I at each pixel, d_i, is then used to correct the initial guess function and to check whether the iteration process converges to a satisfactory solution. The summation of the absolute values of d_i of all pixels can be regarded as a criterion of satisfactory solution. Before the criterion is reached, I'_i is subtracted by cd_i at each pixel to obtain a new function I''', where N is the pixel number and c is an adjustable parameter used to control the degree of correction of I'. In the operation, the choice of an appropriate c value is crucial. The iteration procedure may not converge to a satisfactory solution if c is too large. The result of a particular iteration is obtained by selecting the positive values of I'''_i and setting others at 0 because negative intensity is unreasonable. This result is used as the guess function of the next iteration. The process is terminated when a satisfactory solution is achieved.

4. Numerical Simulations

To demonstrate the capabilities and estimate the limita-

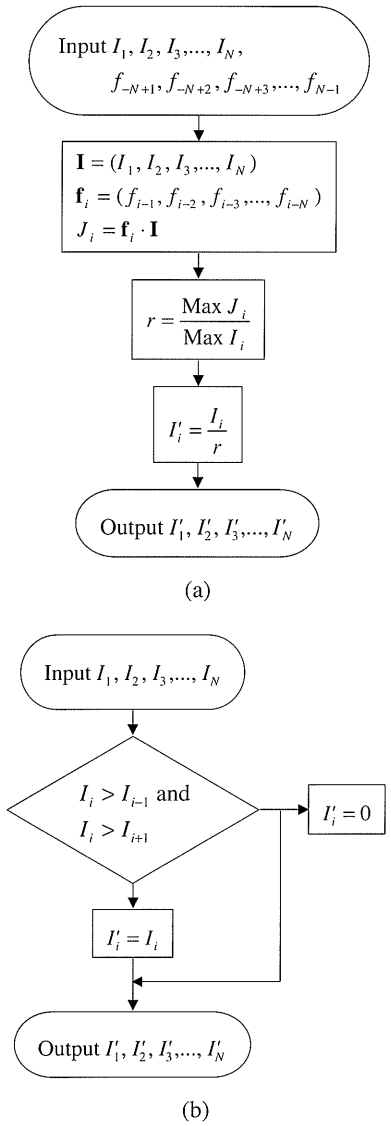

Fig. 1. Flowcharts showing the procedures of constructing the initial guess functions with (a) the first method and (b) the second method.

tions of the proposed algorithms, we use the iteration procedures for simulating the imaging operation of an assumed sample structure with six interfaces, as shown in Fig. 3(a). Here, the separations between two neighboring interfaces range from 1 to 5 μm. Such a sample structure is scanned with an OCT system with the spectral distribution of the light source described in Eq. (7). The center frequency ω_0 is assumed to be 2.355×10^{15} Hz, which corresponds to the center wavelength of 800 nm. The full-width at half maximum (FWHM) of the spectrum was chosen to be 100 nm by setting $\Delta\omega = 0.176 \times 10^{15}$ Hz. Under these conditions, the FWHM of the interference fringe envelope of a single-facet reflection can be calculated through the equation

$$\Delta z = \frac{2\ln 2}{\pi}\frac{\lambda_0^2}{\Delta\lambda} \tag{10}$$

to obtain $\Delta z = 2.84\,\mu\text{m}$. This value is conventionally regarded as the longitudinal resolution of the OCT system. In simulation, the detected signal for the assumed sample

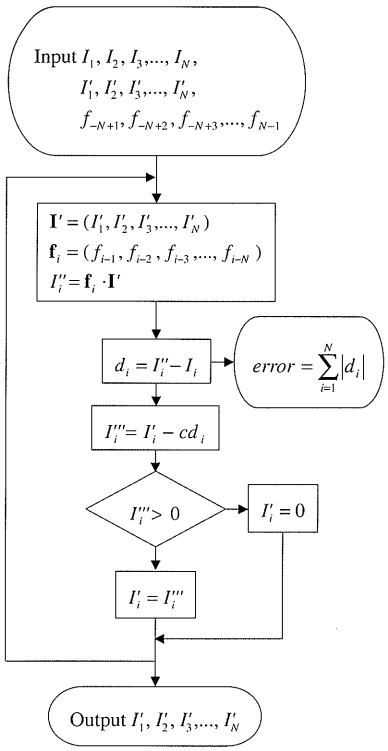

Fig. 2. Flowchart showing the retrieval iteration procedure.

structure can be calculated through Eq. (6) or (8) and is shown in Fig. 3(b). The corresponding one-dimensional OCT image is obtained by demodulating the detected signal and is shown in Fig. 3(c). One can see that the individual interfaces can be well identified when the separation between two neighboring interfaces is larger than 3 μm. When the separation is smaller than 2 μm, the interfering signals resulting from different interfaces overlap each other. Hence, the positions of the interfaces can no longer be correctly identified.

The signals were processed with the proposed algorithms. Figure 3(d) shows the processed results with the first method after 10 (dotted curves) and 100 (solid curves) iterations, respectively. When the separation between two neighboring interfaces is larger than 3 μm, the width of each envelope becomes smaller, corresponding to the contrast enhancement of the image. When the separation is smaller than 2 μm, the original interfaces cannot be retrieved. Figure 3(e) shows the processed result with the second method after 10 iterations. In this situation, the retrieved result looks better when the interface separation is larger than 3 μm. The interfaces with separations smaller than 2 μm cannot be retrieved with the second method either. In both methods, the processed signals approach the convergent results after 10 iterations when the parameter c is set at 0.02. The limitation of the proposed algorithms was estimated by considering a two-interface structure. From the raw data of OCT image, we cannot distinguish the two interfaces or correctly identify their positions when the separation is less than 3 μm. Figures 4(a) and (b) show the simulated signal and its envelope of the two-interface structure with 2 μm in spacing. The interference fringe patterns from the two interfaces overlap each other and

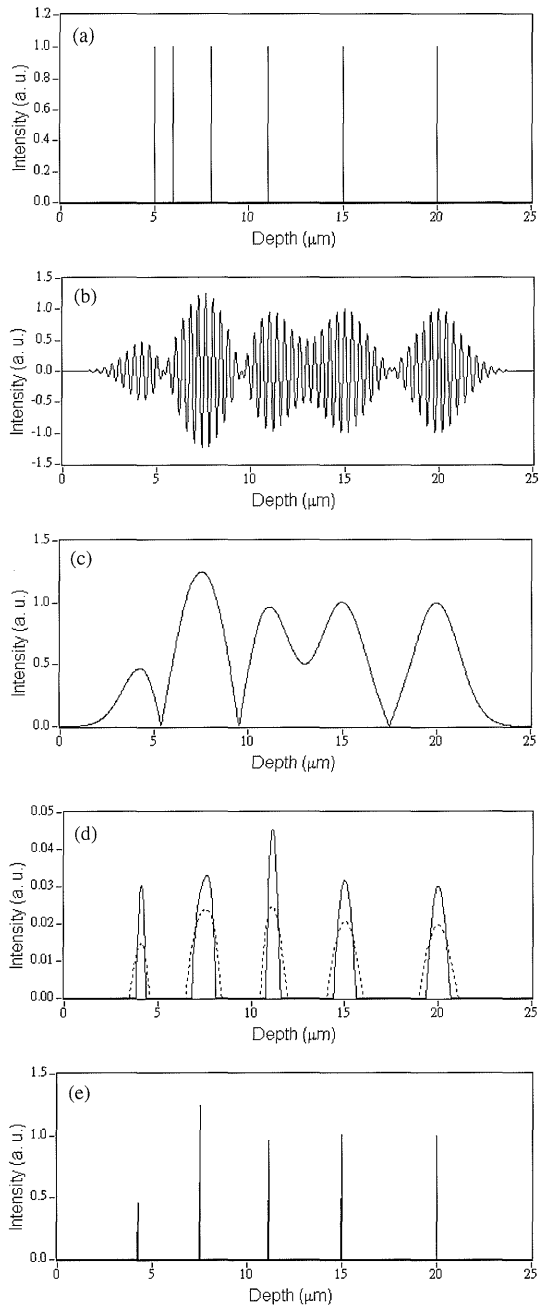

Fig. 3. (a) Assumed sample structure with six interfaces. (b) The simulated detected signal from the assumed sample structure and (c) its fringe envelope. (d) The processed results with the first method after 10 (dotted curves) and 100 (solid curves) iterations. (e) The processed result with the second method after 10 iterations.

cannot be distinguished. The processed results after 10 and 100 iterations with the first method are shown in Fig. 4(c) (dotted curve for 10 iterations and solid curve for 100 iterations). The two interfaces become distinguishable and their positions can be correctly identified after the retrieval process. This means that the longitudinal resolution can be improved with the proposed algorithms if the image feature separation is not much smaller than the resolution cell size. We have found that the two interfaces can be well resolved if the interface separation is larger than 0.8 μm, although their positions might not be correctly identified.

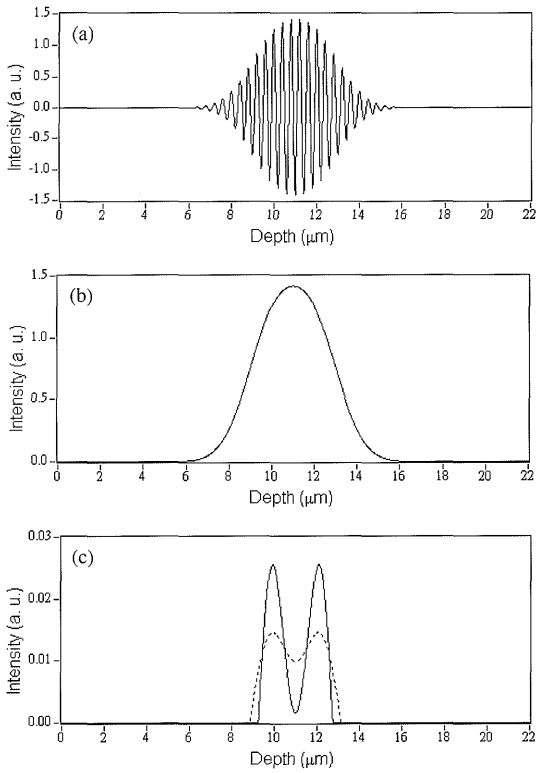

Fig. 4. (a) The simulated interfering signal and (b) its fringe envelope of a two-interface structure with 2 μm spacing. (c) The processed results after 10 (dotted curves) and 100 (solid curves) iterations by the first method.

5. Experimental Results

In experiments, we used a typical free-space OCT system with a mode-locked Ti:sapphire laser (Femtosource) as its light source to scan various samples. The light source provides a non-Gaussian spectrum with the spectral width of about 80 nm. Figure 5(a) shows the one-dimensional OCT image of a human buccal mucosa sample. Before the retrieval procedure, the raw data were smoothed through a low-pass filter to eliminate the high-frequency noise. Figure 5(b) shows the image of filtered data. This set of data was then processed by the first method. The processed image after 10 iterations is shown in Fig. 5(c). One can see that not only does the front boundary become sharper, but also the sample structure becomes clearer, and the image contrast is significantly enhanced.

Figure 6(a) shows a two-dimensional OCT image of the same sample. Figure 6(b) shows the same image after low-pass filtering. The image after processing with 10 iterations of the first method is shown in Fig. 6(c). Here, we can easily distinguish the layered structures including the (i) keratin, (ii) epithelium, (iii) connective tissue and (iv) salivary glands, as indicated in the figure. The image contrast was significantly enhanced and the boundaries between the layers are clearer.

6. Conclusions

In conclusion, we have proposed two process algorithms to retrieve the sample structure and enhance the image contrast in OCT images. Based on the concept of deconvolution, we

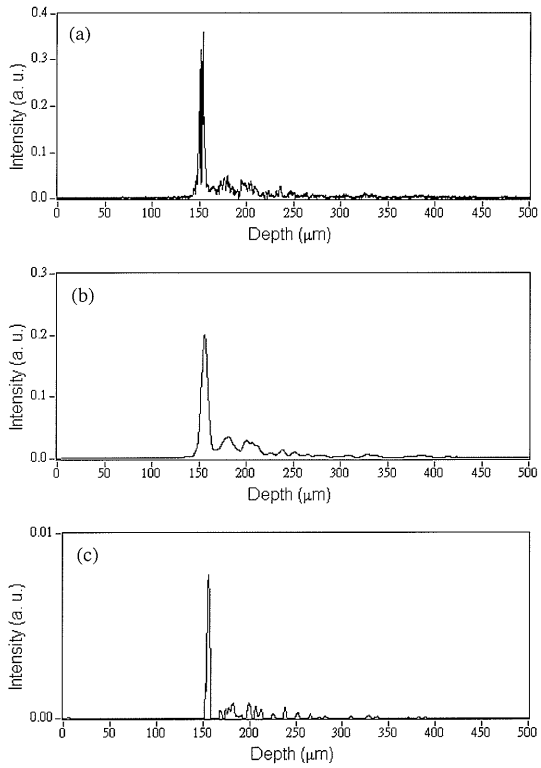

Fig. 5. One-dimensional backward-scattered intensity distribution in the OCT image of a human buccal mucosa sample: (a) before the low-pass filter, (b) after the low-pass filter, and (c) after 10 iterations with the first method.

used the methods of iteration to approach the real structure of the sample. The effects of the process algorithms were demonstrated with numerical simulations and real OCT scanning images. The application limitation of the algorithms was also examined. In real OCT operation, a human buccal mucosa sample was scanned with a free-space OCT system. After processing with the proposed algorithm, the sample structure became clearer and the image contrast was significantly enhanced.

Acknowledgement

This research was supported by the National Health Research Institute of The Republic of China, under the grant NHRI-EX92-9220EI.

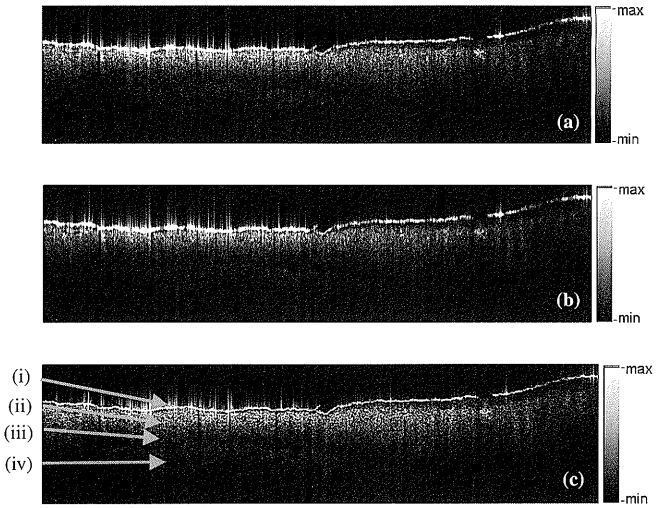

Fig. 6. Two-dimensional OCT images of the human buccal mucosa sample (2 mm × 0.5 mm): (a) before the low-pass filter, (b) after the low-pass filter, and (c) after 10 iterations with the first method.

References

1) D. Huang, E. A. Swanson, C. P. Lin, J. S. Schuman, W. G. Stinson, W. Chang, M. R. Hee, T. Flotte, K. Gregory, C. A. Puliafito and J. G. Fujimoto: Science **254** (1991) 1178.
2) B. Povazay, K. Bizheva, A. Unterhuber, B. Hermann, H. Sattmann, A. F. Fercher, W. Drexler, A. Apolonski, W. J. Wadsworth, J. C. Knight, P. St. J. Russel, M. Vetterlein and E. Scherzer: Opt. Lett. **27** (2002) 1800.
3) Y. Wang, Y. Zhao, J. S. Nelson, Z. Chen and R. S. Windeler: Opt. Lett. **28** (2003) 182.
4) D. L. Marks, A. L. Oldenburg, J. J. Reynolds and S. A. Boppart: Opt. Lett. **27** (2002) 2010.
5) A. M. Kowalevicz, T. Ko, I. Hartl, J. G. Fujimoto, M. Pollnau and R. P. Salathé: Opt. Express **10** (2002) 349.
6) M. D. Kulkarni, C. W. Thomas and J. A. Izatt: Electron. Lett. **33** (1997) 1365.
7) M. Bashkansky, M. D. Duncan and J. Reintjes: App. Opt. **37** (1998) 8137.
8) I. J. Hsu, C. W. Sun, C. W. Lu, C. C. Yang, C. P. Chiang and C. W. Lin: Appl. Opt. **42** (2003) 227.
9) R. Tripathi, N. Nassif, J. S. Nelson, B. H. Park and J. F. de Boer: Opt. Lett. **27** (2002) 406.